UCRL-JRNL-233986

Irreversible volume growth in polymer-bonded powder systems: effects of crystalline anisotropy, particle size distribution, and binder strength

Amitesh Maiti, Richard H. Gee, D. Mark Hoffman, Laurence E. Fried

August 24, 2007

Disclaimer

This document was prepared as an account of work sponsored by an agency of the United States government. Neither the United States government nor Lawrence Livermore National Security, LLC, nor any of their employees makes any warranty, expressed or implied, or assumes any legal liability or responsibility for the accuracy, completeness, or usefulness of any information, apparatus, product, or process disclosed, or represents that its use would not infringe privately owned rights. Reference herein to any specific commercial product, process, or service by trade name, trademark, manufacturer, or otherwise does not necessarily constitute or imply its endorsement, recommendation, or favoring by the United States government or Lawrence Livermore National Security, LLC. The views and opinions of authors expressed herein do not necessarily state or reflect those of the United States government or Lawrence Livermore National Security, LLC, and shall not be used for advertising or product endorsement purposes.

Irreversible volume growth in polymer-bonded powder systems: effects of crystalline anisotropy, particle size distribution, and binder strength

Amitesh Maiti, Richard H. Gee, D. Mark Hoffman, and Laurence E. Fried

Lawrence Livermore National Laboratory, Livermore, CA 94551

Abstract

Pressed-powdered crystallites of intrinsically anisotropic materials have been shown to undergo irreversible volume expansion when subjected to repeated cycles of heating and cooling. We develop a coarse-grained (micron-scale) interaction Hamiltonian for this system and perform molecular dynamics simulations, which quantitatively reproduce the experimentally observed irreversible growth. The functional form and values of the interaction parameters at the coarse-grained level are motivated by our knowledge at the atomic/molecular scale, and allows a simple way to incorporate the effect of polymeric binder. We demonstrate that irreversible growth happens only in the presence of intrinsic crystalline anisotropy of the powder material, is mediated by particles much smaller than the average crystallite size, and can be significantly reduced in the presence of high-strength polymeric binder with elevated glass transition temperatures.

I. Introduction

Standard simulation methods in materials science and engineering can be roughly classified into three groups: (1) atomic-level molecular dynamics or Monte Carlo, based on forces obtained from quantum mechanics or classical potentials; (2) continuum-scale finite-elements modeling, which could be grid or particle based; (3) an emerging field of mesoscale modeling, aimed at analyzing phenomena at intermediate length and time-scales. Although many challenges still remain, the first two simulation methods are quite mature. In comparison, serious inroads into mesoscale methods have started relatively recently, being prompted by new problems in composite science, geophysics, biomaterials, and diverse applications of nanotechnology.

Even within the field of mesoscale modeling there are application areas where the methodology is more developed than others. This is particularly true for "soft" materials like simple molecular liquids to complex polymeric fluids, blends, and melts where statistical mechanical theories have led to fairly robust algorithms based on classical density functionals [1-3] and bead-spring models [4-6]. However, examples abound where such methodologies are not readily applicable, e.g., biomaterials like bone and teeth composed of ceramic crystallites within a soft protein-like matrix [7], or shells (e.g., nacre) comprising brick-and-mortar like arrangement of aragonite crystals with very little soft matrix [7], or geological systems like the earth's crust consisting of plates floating on a relatively softer mantle [8], or composites where clay nanoparticles are embedded within a predominantly soft polymeric environment [9], or plastic-bonded explosives where crystallites of high-energy molecules are bonded with a small amount of polymeric binder [10]. The presence of a "hard" component in the preceding examples creates several modeling challenges: (1) hardness in potential may result in a reduction of the effective time-step, which can severely limit timescale of phenomena to be studied; (2) in the absence of general guiding principles, e.g., an equivalent of the Flory-Huggins theory [11] for hard systems accurate mesoscale parameters would typically require well-characterized experimental data on individual components as well as their interactions, which may not be readily available.

In this paper we consider the specific example of a plastic-bonded explosive (PBX) consisting of a pressed powder of the energetic material 1, 3, 5-triamino-2, 4, 6-trinitrobenzene (TATB) bonded by a small amount (~ 5-7.5% by weight) of polymer [12]. The single-crystal of TATB in its predominant

polymorphic form has a layered structure (like graphite), and pressed powder TATB explosives, with or without polymer binder has previously been found to undergo the interesting phenomenon of irreversible growth upon repeated cycles of cooling and heating [12]. Irreversible growth is also found to occur in other anisotropic materials like boron-nitride and graphite [13]. The phenomenon of irreversible growth is remarkably contradictory to common intuition by which one expects to see a lowering of system energy through gradual compaction of the powder [14]. Our challenge was to develop a mesoscale model that describes the essential interactions at the micron scale, and is able to reproduce the irreversible growth phenomenon with quantitative accuracy.

II. Experimental details

In order to obtain a consistent set of quantitatively accurate data, we performed careful thermometric analysis on well-prepared samples in which TATB particles were bonded with a few % of polymeric binder. In the currently existing formulations a 3:1 copolymer of cholorotrifluoroethylene and vinylidine fluoride, called Kel-F-800 [12] (ρ =2.00 g/cc) was used as the binder. However, because of low glass transition temperature ($T_g \sim$ 22-34 °C) of Kel-F-800, such a binder can lead to significant irreversible growth, as shown below. To reduce irreversible growth, we have recently formulated TATB-PBX with fluoropolymers of high density and high glass-transition temperature (T_g)[15]. One such polymer with good binder properties is Cytop (ρ =2.03 g/cc, $T_g \sim$ 108 °C). Molecular structures of both Cytop and Kel-F-800 monomers are described in ref. [15].

The linear expansion data was obtained by a thermo-mechanical analyzer (TA instruments, model 2940) using a cylindrical sample of about 6.35 mm diameter and 6.62 mm length, which was compression molded with considerable care taken to ensure that the ends were flat and parallel. The temperature was cycled within a range of approximately -54 to +74 ºC at a ramp rate of 3 °C/min. Fig. 1(a) displays, for one specific Kel-F-800-bonded sample (marked "KelF #2") the variation of length as a function of temperature for the first 12 thermal cycles, with the room temperature values (on the cooling part of the cycle) indicated by filled circles. The irreversible growth for this sample is ~ 0.3% through the first 12 cycles. Fig. 1(b) re-plots the room temperature length of sample KelF #2 as a function of thermal cycle, along with the same measurement for two other Kel-F-800 samples (KelF #1

and #3) and that of a recently formulated sample with the Cytop binder [15]. From Fig. 1(b) one immediately observes that: (1) even for the three KelF samples there is a strong sample-to-sample variation of the amount of irreversible growth. This is likely due to differences in the density composition (i.e. particle size-distribution) of the powder and/or possible differences in orientational alignment of the particles relative to their basal planes, caused by different parts of the billet being subjected to different stress fields during the pressing process; (2) irreversible growth in samples formulated with the cytop binder is an order of magnitude smaller, although the length variation as a function of thermal cycle is not as smoothly monotonic as for the KelF samples. In the rest of the paper we develop a coarse-grained model that is able to provide a realistic representation of the underlying process that leads to the irreversible volume growth. We show that rationally motivated interaction parameters can quantitatively reproduce the behaviors of Fig. 1. In the process we uncover the important driving forces and mechanism behind the irreversible growth, and determine a correlation between the coarse-grained interaction parameters and the properties of the polymeric binder. The essential features of this model were described in a recent letter publication [16]. The purpose of the present paper is to provide more detailed justification of the parameter values, the size-scaling behavior of various quantities, and an analysis of irreversible growth in terms of particle movement.

Before the modeling discussions we should note that although the amounts of irreversible growth in Fig. 1 appear to be only a fraction of a percent or smaller, all this growth implies increased "void" volume. In reality, the PBX material is compressed to a very high density, as high as 98% of the theoretical maximum density. This implies a total void volume of only $\sim 2\%$. Thus, a 1% irreversible increase in sample volume represents a 50% increase in the total void volume. Considering that these voids act as "hot spots" during detonation processes [17], one could appreciate the impact of altering the irreversible growth even by a few tenths of a percent.

III. Model construction

Atomistic: Experimentally TATB is a layered structure with triclinic space group P-1 [18]. The basic unit cell is displayed in Fig. 2(a), with strong inter-molecular hydrogen bonds (Fig. 2(b)) within layers parallel to the XY plane. The hydrogen-bonds lead to significant anisotropy when comparing

4

properties within and perpendicular to the layers [19]. In particular, the coefficient of thermal expansion (CTE) is significantly larger perpendicular to the layers as compared to within the layers [19, 20]. In order to determine the average particle shape, we computed the equilibrium morphology (Fig. 2(c)) of crystalline TATB by minimizing total surface energy [21] of the original molecular crystal under the constraint of a fixed volume. This is accomplished by the Wulff construction procedure [22] as automated in the Morphology module [23] from Accelrys. For the surface energy calculations we employed an accurate inter-atomic potential developed for TATB [24].

Coarse-graining: Typical TATB particle size in such powder materials varies between a micron to several hundred microns. Thus, a natural choice for us was to coarse-grain a micron-sized cubic block of TATB crystal into a single mesoscale TATB "bead". From the convenience of symmetry we selected the orientation in which the edges of the cube (defining a bead) were parallel to the X, Y and Z axes of the underlying atomic lattice. Fig. 3(a) displays a periodic supercell representation of the coarse-grained or "meso" TATB crystal. In order to incorporate the intrinsic crystalline anisotropy of the atomic lattice we designated meso beads in alternate layers parallel to the XY plane (see Fig. 2(a)) as "A" and "B" beads, and differentiated between like (*i.e.*, A-A and B-B) and unlike (*i.e.*, A-B) bonds through different values of the thermal expansion coefficients (*i.e.*, $C^{Th}_{AA} = C^{Th}_{BB} \neq C^{Th}_{AB}$, see section IV). Fig. 3(b) displays a meso representation of crystallites of the same shape as the computed morphology (Fig. 2(c)) by cleaving appropriate planes from the meso crystal model of Fig. 3(a). It should be noted that the Morphology theory only yields the average shape but not the size of crystallites [23]. Thus, in general it is necessary to build an ensemble of meso particles of various sizes to create a proper representation of a powdered material. Fig. 4 displays a representative example of several ensembles used in our simulations. Fig. 4(a) illustrates an ensemble consisting only of larger crystallite particles, which is an inefficiently packed system with a significant amount of void space. Fig. 4(b), in which inter-crystallite voids of Fig. 4(a) are packed with small TATB particles (represented by small cubes), is a much more realistic representation of an experimental pressed powder system, where high pressure is employed to achieve a density as high as 98% of the theoretical maximum. It is important to note that such a high experimental packing density can only be achieved through the presence of small particles, either present originally in the sample, or created by breaking of larger crystallites under pressure. Hereafter, we refer to structures in Fig. 4(b) as a *pressed-powder*. To create such structures we use a random packing program in which we first decide on a size

distribution of crystallites, and pack starting from the biggest particles, and progressively go down in size, and finally fill inter-crystallite space with the smallest cubes in order to achieve the experimental packing fraction. In the plastic-bonded material (PBX) there is an additional component, i.e., the polymeric binder, which is known to form thin coats around the TATB particles. One possible representation of the polymer could be through single "polymer beads" in the inter-crystalline spaces (shown schematically by red balls in Fig. 4(c)). However, from explicit simulations we found that such a representation can lead to an artificial inhomogeneity of polymer distribution due to spatial non-uniformity of polymer bead density, while the introduction of an additional component adds an unnecessary burden to interaction parameterization. A much simpler way to represent the thin polymeric component, which overcomes both the above problems, was through suitable modification of inter-crystallite interaction potential, as discussed below.

As we found from the experimental section, the amount of irreversible growth has a strong sample-to-sample variation, even within PBX using the same binder (see KelF #1, #2 and #3 in Fig. 1(b)). To model such variation, we created a few different particle distributions. Fig. 4(d) displays a pressed powder model that is different from that of Fig. 4(b). Structures in Fig. 4(b) and 4(d) differ not only in the overall ratio of large to small particles (small particles comprising roughly 45% in Figs. 4(b) and 30% in Fig. 4(d)), but also in the relative orientation of the larger crystallites. As we will see in the next section, such differences indeed lead to different amounts of irreversible growth.

IV. Mesoscale interactions

Although no formal theory of irreversible growth in anisotropic material exists in the literature, there have been a few suggested mechanisms, including the excitation of libration modes, and build-up of high internal pressures, both of which can potentially lead to intra-crystalline voids [12, 19]. In the temperature range of our interest (-54 to 74 °C) the libration mechanism is unlikely, as is supported by atomistic simulations using a recently-developed forcefield [24], as well as X-ray observations [18]. We, therefore, explore a mechanism in which each crystallite can vibrate, translate, and rotate, but otherwise has its shape and size intact upon thermal cycling. Such a mechanism is natural given that the intra-crystallite bonding interactions are much stronger than the inter-crystallite nonbond

interaction between two external surfaces. For bead-bead interaction *within* a meso-crystallite we chose explicit nearest-neighbor bond and angle-energy terms in the simple *harmonic* form:

$$E(b_{\alpha\beta}) = K_{bond}(b_{\alpha\beta} - b^0{}_{\alpha\beta})^2 \text{, and } E(\theta_{\alpha\beta\gamma}) = K_{angle}(\theta_{\alpha\beta\gamma} - \theta^0{}_{\alpha\beta\gamma})^2 \text{,} \qquad (1)$$

where each of the subscripts α, β, γ could be bead types *A* or *B*, while the weaker *inter-crystallite* bead-bead interaction was chosen to be of the Morse functional form:

$$E(r_{ij}) = D[\{1 - e^{-\alpha(r_{ij} - r_0)}\}^2 - 1] \qquad (2)$$

The Morse function is sharper and more localized than the more commonly used Lennard-Jones 6-12, and is therefore more appropriate for describing the hard interaction between the surfaces of solid crystallites representing the powdered material. The hope was that the effectiveness of the polymer binder in controlling irreversible growth would be adequately captured by the two interaction parameters D and α of Eq. (2), which basically control the *depth* and the *inverse range* of the inter-crystalline interactions, respectively. We will revisit this issue in section V when we compare simulation results of irreversible growth with experimental values.

Due to the absence of anharmonicity in the bond terms in Eq. (1), we incorporated thermal expansion by making the equilibrium bond separation T-dependent, i.e.,

$$b^0{}_{\alpha\beta}(T) = b^0{}_{\alpha\beta}(T_L) + C^{Th}{}_{\alpha\beta}(T - T_L) \text{,} \qquad (3)$$

where $T_L (= -54 \,^{\circ}\text{C})$ is the lower limit of the temperature range of our interest, and $C^{Th}{}_{\alpha\beta}$ is the experimentally measured CTE. Because of previously-stated anisotropy of TATB, the in-plane CTE ($C^{Th}{}_{AA} = C^{Th}{}_{BB}$) is much smaller than the CTE perpendicular to the basal planes ($C^{Th}{}_{AB}$) [25].

Table 1 lists the values of various parameters defined in Eqs. (1-3) and how they scale with bead-size N [26]. Large crystallites in our experimental samples are of dimensions several tens to several hundreds of μm, which sets the basic length-scale, governed by b^0, to 1 μm. The parameter K_{bond} is chosen to ensure that the amplitude of oscillation $\sim \sqrt{k_B T / K_{bond}}$ is a small fraction (i.e. < 8%) of the inter-bead distance. The same logic holds for K_{angle}. Our choice makes the fastest oscillation time $\tau_{fastest}$ $\sim 2\pi / \sqrt{K_{bond}} = 0.6$ in reduced units. At the atomistic scale $\tau_{fastest} \sim 10^{-13}\text{-}10^{-12}$ *s*. Thus, at our

mesoscale $\tau_{fastest} \sim 10^{-3} - 10^{-2}$ s (using the $N^{5/6}$ scaling [26]). The MD time-step used is two orders of magnitude smaller than $\tau_{fastest}$. As for the Morse parameters, the inter-crystalline r_0 is chosen as slightly (i.e., 30%) larger than the intra-crystalline b^0, while the Morse parameters α and D are chosen such that they satisfy the constraints: (1) $D \ll K_{bond}(b^0)^2$, (2) $\delta \sim \sqrt{k_B T / D\alpha^2} \ll r_0$, and (3) $D \gg k_B T$, corresponding to the requirements that: (1) inter-crystallite interactions are much weaker than intra-crystallite interactions, (2) external surfaces do not approach to within a distance $(r_0 - \delta)$, where δ is a very small fraction of r_0, and (3) the cohesive energy maintains a proper physical density under ambient conditions. To satisfy conditions (1) and (3), we borrowed from the familiar concepts of molecular interactions, and chose D of the order of a hydrogen bond $\sim$ 7-10 kcal/mol. To satisfy condition (2), we explored a few values in the range α = 10-60 μm^{-1}, corresponding to $\delta/r_0 \sim 3\%$ or less. Larger values of α did not seem to affect the amount of irreversible growth [16].

V. Simulation details and results

Using the bead-bead potential defined in the previous section we carried out classical molecular dynamics simulations using the LAMMPS code [27]. The smoothness of the experimental curves as exemplified in Fig. 1(a) results from averaging over a macroscopically large number of crystallites within a real sample. Mimicking such behavior necessitated substantially large computational cells as well. We considered simulation cells with total bead number in the range 50000-100000, with the lower end corresponding to structures like Fig. 4(a) (with significant void space) and the upper end corresponding to pressed-powder systems (e.g., Figs. 4(b) and 4(d)). Each simulation was carried out in two stages:

1. Equilibration: This initial stage was to ensure that all inter-particle void space was squeezed out as efficiently as possible, i.e., in other words to enable the sample to reach its highest possible packing density. To this end, we subjected the initially constructed pressed-powder samples to long NPT dynamics simulations (10^7-10^8 steps) at somewhat elevated temperatures (1000 K or higher), followed by gradual cooling to T_L = -54 °C, the low temperature of the experimental thermal cycles. During this entire annealing procedure the bond-lengths were not varied according to Eq. (3), but rather fixed at

their low-temperature value $b_{\alpha\beta}{}^0(T_L)$. At the end of the equilibration run we computed the inter-particle void space using a "hard sphere" radius of $r_0/2$ for each meso bead (where r_0 is the inter-crystalline Morse function parameter, see Eq. (2)). We repeated the above procedure several times to observe that the void volume decreases progressively for the first few equilibration cycles, and then saturates at a value of 2-4% of the total volume of the simulation cell (corresponding to 96-98% packing density).

2. Thermal cycling: In this stage, the efficiently packed annealed sample was subjected to several (8-12) thermal cycles. Each cycle consisted of raising the temperature from the low (-54 °C) to the high (74 °C) temperature in 7 steps, and then lowering the temperature reversibly in another 7 steps. At each temperature step the bond-lengths were expanded according to Eq. (3), and NPT dynamics was performed for 10^6 steps.

We performed the above simulation procedure for several different ensembles over a range of interaction parameters D and α. Simulation results on structures in Figs. 4(b) and 4(d) are displayed in Fig. 5. Fig. 5(a) considers fixed values of the interaction parameters, i.e., $D=7$ and $\alpha=40$ and explores two effects on irreversible growth: (1) sample dependence, and (2) the effect of intrinsic crystalline anisotropy. That the amount of irreversible growth has a strong dependence on the sample is clear from the differences in the two curves marked by the phrase "anisotropic" – the growth is higher for sample Fig. 4(d) than for Fig. 4(b). These structures differ both in particle size composition as well as the relative orientation of the larger particles. Unfortunately, from just these two curves we cannot comment on how irreversible growth behaves as a function of, say, small particle fraction. Even a rough qualitative description of the dependence of irreversible growth on size distribution or orientation demands a rather large number of simulations on many different samples, an endeavor beyond the scope of our project. However, the difference in irreversible growth between the two samples is in clear agreement with the difference between the three KelF curves in the experimental Fig. 1(b).

Investigating the importance of crystalline anisotropy to irreversible growth was much simpler. For this, we simply considered an isotropic crystal, i.e., $C^{Th}{}_{AA} = C^{Th}{}_{BB} = C^{Th}{}_{AB}$ [28]. From Fig. 5(a), one immediately recognizes that the irreversible growth (for the same sample) becomes much smaller

in the absence of crystalline anisotropy, which clearly explains why such volume growth is associated only with intrinsically anisotropic materials [12, 13]. A physical picture of irreversible growth in terms of particle displacement driven by crystalline anisotropy is discussed later.

In Fig. 5(b) we concentrate on one particular sample (structure of Fig. 4(d)) and vary the inter-crystallite interaction parameters (i.e., Morse parameters D and α, see eq. (2)) so as to reproduce the effect of the polymeric binder on irreversible growth. More specifically, we wanted to see if we could explain an order of magnitude smaller irreversible growth for cytop-bound TATB-PBX as compared with the traditional samples bound by KelF-800. Atomic-scale molecular dynamics simulations suggest that Cytop and KelF have quantitatively similar interfacial binding and wetting properties of TATB [15], which implies similar values of the D parameter for these binders. However, the main difference (that led us to explore Cytop in the first place) is where the glass transition temperature T_g of the binder lies with respect to the upper thermal cycle limit (UTCL) of 74 °C. Thus for KelF the T_g is 40-50 °C below UTCL, while that for Cytop it is 30-40 °C higher than UTCL [15]. This would imply that at the upper part of the thermal cycle, where the inter-crystallite thermal displacements are the largest, a cytop-bonded PBX would still feel a strong restoration force back to the initial configuration. In contrast, in a KelF-bonded PBX at these high temperatures the binder would be above its T_g, and the TATB particles would be weakly interacting with each other. A simple way to represent the above behavior in our mesoscale model would be to use a smaller value of the α parameter for a cytop-bonded system, which increases the inter-particle interaction *range* and effectively allows particles to remain bonded even through large relative displacements. To summarize, an appropriate representation of the two binders in our mesoscale model would be to use the same value of D, but a smaller value of α for Cytop as compared to KelF.

Fig. 5(b) displays our simulation results on sample Fig. 4(d) in which we kept the parameter D constant ($D=7$) and varied only α. From these simulations we find that, for this particular sample the irreversible growth with the cytop binder (see Fig. 1(b)) can be quantitatively matched by using $\alpha=10$, while that for the KelF-bound PBX samples need a larger α (20 or higher). Ideally, we would like to match a value of (D, α) set to a given binder. However, that would require us to mimick the actual particle-size and orientational distribution of the real samples in our simulation samples. Unfortunately, we do not have enough experimental characterization data to perform such a detailed procedure. In

10

spite of the above limitation, it was encouraging to see the effect of irreversible growth on the parameter α, and the fact that it was in agreement with our intuition regarding T_g and polymer stiffness. We also performed limited simulations with a different value of parameter D (=10) and found that the dependence of irreversible growth on α is much less pronounced [16], which perhaps indicates that the model is useful only in a narrow range of values for D around 7.

Finally, in order to decipher a physical mechanism behind irreversible growth, we carried out an analysis of structures before and after thermal cycling, and kept track of the displacement of each bead during the process. Fig. 6 plots a frequency distribution of the number of beads as a function of the net amount of displacement after the first 12 thermal cycles in the simulation represented by the uppermost curve of Fig. 5(a) (i.e., structure of Fig. 4(d) with crystalline anisotropy). One observes that in general the smaller particles get displaced more than the larger particles. To isolate the effect of the smaller particles we carried out simulations under crystalline anisotropy with larger particles only (e.g., see Fig. 4(a)), and observed that there is no significant irreversible growth (i.e., the curve was similar to the lowermost curve of Fig. 5(a)). This result, along with Fig. 6 together seem to suggest the following mechanical picture: the irreversible growth happens by the movement of crystallites induced by anisotropic stress build up due to intrinsic crystalline anisotropy. In the isotropic case, all crystallites expand by the same fractional amount in all directions, and there is little residual stress that can drive volume growth. Anisotropy-generated local stress, in contrast, tends to drive crystallites from an initial pressed-powder configuration to one of a large number of metastable states with slightly less compaction density. Such structures are of slightly higher energy than the original compacted configuration, but likely with higher configurational entropy. Due to the facetted particle shapes, such a movement is possible only in the presence of small particles, which effectively act as lubricants and allow the system to move out of the compacted geometry and explore the metastable phase space. In their absence, the crystallites get jammed [29], and there is no volume growth. Gravity-induced pressure-nonuniformity have previously been observed to lead to irreversible growth in a column of glass spheres subjected to thermal cycles [30], and such behavior analyzed with a simple model [31]. Entropic affects have also been attributed to irreversible growth in polycarbonate compacts [32].

VI. Conclusions

In summary, we have developed a mesoscale model for a pressed-powder system, which naturally extends simulation length-scales to *microns* and time-scale to *seconds*. Through appropriate parameter choice the method quantitatively reproduces the phenomenon of irreversible growth under repeated thermal cycles. It provides a clear demonstration that irreversible growth happens only in the presence of intrinsic crystalline anisotropy. It also generates the important insight that such growth is mediated by particles much smaller than the average crystallite size. Finally, the method constitutes a simple parametric way to investigate the effect of polymer binder on powder morphology and growth. In particular, an order-of-magnitude reduction in irreversible growth in the presence of a high-T_g high-strength fluoropolymer (cytop) can be represented with an appropriate reduction of the interaction parameter α. Preliminary simulations also indicate the same total irreversible volume growth even when the system is mechanically confined in one of the dimensions, in agreement with limited experimental data. It would be ideal to map out the amount of irreversible growth as a function of large-to-small-particle ratio. Unfortunately, such a characterization is complicated by a strong dependence on the relative initial orientation of the large particles. We could thus carry out detailed study only on a handful of simulation samples. Our approach is formally more similar to an atomistic force field than the particle-based approaches that have been previously used to study continuum flow problems, e.g., smoothed particle hydrodynamics (SPH) [33], or its derivative, smooth particle applied mechanics (SPAM) [34]. Another reasonable alternative might be to adopt a finite-elements-based approach [35]. Multiple method possibilities notwithstanding, we believe that the methodology developed here is general and robust, and should be useful in simulating the structural evolution of important materials systems in diverse science and engineering disciplines.

References:

1. J.G.E.M. Fraaije, et al. *J. Chem. Phys.* **106**, 4260 (1997).

2. G. H. Fredrickson, V. Ganesan, and F. Drolet, *Macromolecules* **35**, 16 (2002).

3. S. C. Glotzer and W. Paul, *Annu. Rev. Matter. Res.* **32**, 401 (2002).

4. R. D. Groot and P. B. Warren, *J. Chem. Phys.* **107**, 4423 (1997).

5. A. Maiti, J. Wescott, and G. Golbeck-Wood, *Int. J. Nanotechnology* **2**, 198 (2005).

6. M. Karttunen, I. Vattulainen, A. Lukkarinen, eds. *Novel Methods in Soft Matter Simulations*, Lecture Notes in Physics 640, Springer-Verlag, Berlin, Heidelberg (2004).

7. H. Gao, B. Ji, I. L. Jager, E. Arzt, and P. Fratzl, *Proc. Nat. Acad. Sci.* **100**, 5597 (2003), and references therein.

8. K. C. Kondie, *Earth as an evolving planetary system*, Elsevier Academic Press (2005).

9. T. J. Pinnavaia and G. W. Beall, eds., *Polymer-Clay Nanocomposites*, John Wiley & Sons (2000).

10. P. W. Cooper, *Explosives Engineering*, Wiley-VCH (1996).

11. M. Doi, *Introduction to Polymer Physics*, Oxford Science Publications (1996).

12. H. F. Rizzo, J. R. Humphrey, and J. R. Kolb, *Propellants Explos.* **6**, 57 (1981).

13. G. W. Hollenberg and R. Ruh, *AIP Conf. Proc.* **17**, 241 (1973).

14. F. X. Sanchez-Castillo and J. Anwar, *J. Chem. Phys.* **118**, 4636 (2003).

15. R. H. Gee, A. Maiti, S. Bastea, and L. E. Fried, *Macromolecules* **40**, 3422 (2007).

16. R. H. Gee, A. Maiti, and L. E. Fried, *Appl. Phys. Lett.* **70**, 254105 (2007).

17. A. L. Nicols, *AIP Conf. Proc.* **845**, 465 (2006).

18. H. H. Cady and A. C. Larson, *Acta Crystallogr.*, Part 3, **18**, 485 (1965).

19. J. R. Kolb and H. F. Rizzo, *Propellants Explos.* **4**, 10 (1979).

20. Experimentally, the in-plane CTE are $\sim 8 \times 10^{-6}$ /K and 20×10^{-6} /K along the *a* and *b* axes, and $\sim 250 \times 10^{-6}$ /K normal to the basal plane [19].

21. J. W. Gibbs, *Collected Works*, Longman, New York (1928).

22. G. Wulff, *Z. Kristallogr.* **34**, 449 (1901); I. V. Markov, *Crystal Growth for Beginners*, World Scientific, Singapore (1995).

23. See: http://www.accelrys.com/products/mstudio/modeling/crystallization/morphology.html .

24. R. H. Gee et al., *J. Chem. Phys.* **120**, 7059 (2004).

25. In keeping with the experimental CTE values in [20], we used $C^{Th}_{AA} = C^{Th}_{BB} = 14 \times 10^{-6}$ /K, and $C^{Th}_{AB} = 250 \times 10^{-6}$ /K for simulations with crystalline anisotropy.

26. The bead-size *N* is representative of the number of atoms each bead comprises of. Equating bond-length b^0 to the edge of a cubic bead of size *N* implies its $N^{1/3}$ scaling. In our scheme the temperature $k_B T$ and the ratio $\lambda = $ *(bead oscillation amplitude)*$/b^0$ are independent of bead-size *N*. Therefore $K_{bond}(\lambda b^0)^2 \sim k_B T$ implies that K_{bond} scales as $N^{-2/3}$. The fastest oscillation time $\tau_{fastest} \sim \sqrt{M/K_{bond}}$, which implies a scaling of $N^{5/6}$ (given that the bead mass *M* scales linearly with *N*).

27. See webpage: http://www.cs.sandia.gov/~sjplimp/lammps.html.

28. For isotropic simulations we used $C^{Th}_{AA} = C^{Th}_{BB} = C^{Th}_{AB} = 93 \times 10^{-6}$ /K corresponding to the same net volume expansion as in the anisotropic case [25].

29. A. Donev, F. H. Stillinger, and S. Torqauto, *Phys. Rev. Lett.* **95**, 090604 (2005), and references therein.

30. L. Vanel et al., in *Physics of Dry Granular Media*, H. J. Herrmann, J. P. Hovi, and S. Luding (eds.), Kluwer Academic Publishers, Dordrecht, 1998.

31. P-G. de Gennes, *CR Acad. Sci.* (Paris) **327**, 267 (1999).

32. L. W. Vick and R. G. Kander, *Pol. Eng. Sci.* **38,** 1985 (1998).

33. J. Monaghan, *Ann. Rev. Astronomy and Astrophysics* **30**, 543 (1992).

34. W. G. Hoover and H. A. Posch, *Phys. Rev. E* **59**, 1770 (1999).

35. F. Froiio, G. Tomassetti, and I. Vardoulakis, *Int. J. Solid. Struct.* **43**, 7684 (2006).

Table 1. Mesoscale parameters used in our simulations. Basic length and energy units are in μm and $kcal/mol$ respectively. The mass unit is that of a mesoscale TATB bead ~ 1.94x10^{-12} gm, which implies $N \sim 10^{12}$ (in terms of # equivalent H-atoms per mesoscale bead).

Variable	Scaling	Physical Unit	Value
Fastest Oscillation Time ($\tau_{fastest}$)	$N^{5/6}$	1-10 ms	0.6
MD Time-step used	$N^{5/6}$	0.01-0.1 ms	0.006
Room temperature ($k_B T$)	N^0	$kcal/mol$	0.6
K_{bond}	$N^{-2/3}$	$kcal/mol/(\mu m^2)$	100.0
K_{angle}	N^0	$kcal/mol/(rad^2)$	100.0
Eq. bond-length (b^0)	$N^{1/3}$	μm	1.0
Eq. angle (A^0)	N^0	rad	$\pi/2$
Morse-parameter D	N^0	$kcal/mol$	7-10
Morse-parameter α	$N^{1/3}$	μm^{-1}	10-60
Morse parameter r_0	$N^{1/3}$	μm	1.3

Fig 1. Irreversible growth of TATB-PBX upon repeated thermal cycling between -54 °C and 74 °C for four different samples: three extracted from traditional material bonded by the KelF-800 polymer (designated by KelF #1, KelF #2, and KelF #3), and a fourth one from a new system bonded by the fluoropolymer cytop. (a) Plot for one of the samples (KelF #2) showing length variation within each thermal cycle; (b) Cycle-to-cycle variation of room-temperature length for all four samples.

Fig 2. (a) Experimental crystal structure of TATB with two molecules per unit cell; (b) Spatially extended model revealing strong inter-molecular hydrogen bonds within the basal plane (parallel to the XY plane of Fig. 2(a)); (c) Computed equilibrium morphology with exposed facets Miller-indexed. Color scheme: C (gray), N (blue), O(red), H(white).

Fig. 3. (a) An equivalent TATB crystal of "meso" beads, with alternating planes of A and B-beads parallel to the XY plane of Fig. 2(a); (b) A meso TATB crystallite with shape comparable with the morphology of Fig. 2(c).

Fig 4. Sample models of TATB powder with packed crystallites: (a) only large crystallites; (b) *pressed-powder:* large crystallites along with small cubic TATB particles (in green and brown); (c) explicit single polymer "beads" (in red) included; (d) pressed-powder model of a second simulation sample with a different orientation and size distribution of the larger TATB particles. The fraction of large particles (in terms of the number of constituent meso beads) are 53.7% and 61.4% respectively for structures in Fig. 4(b) and Fig. 4(d) respectively. The representative length-scales are indicated on Figs. 4(a) and 4(d).

Fig 5. Mesoscale simulation of irreversible growth of TATB pressed-powder models. Only room-temperature data is shown for clarity. (a) Irreversible growth of structures in Fig. 4(b) and 4(d) in the presence and absence of intrinsic crystalline anisotropy. Used fixed inter-crystalline interaction parameters: $D = 7$ and $\alpha = 40$. (b) Dependence of irreversible growth of the structure in Fig. 4(d) on interaction parameter α (for a fixed value of $D = 7$) in the presence of crystalline anisotropy. Each growth curve in Fig. 5(b) can be identified with an experimental curve in Fig. 1(b).

Fig. 6. Displacement histograms of large and small particles after the structure of Fig. 4(d) was subjected to 12 thermal cycles (initial and final structures at room temperature). The simulation corresponds to the uppermost growth curve of Fig. 5(a).
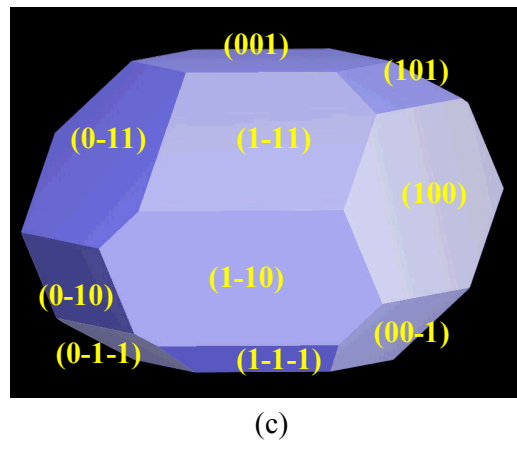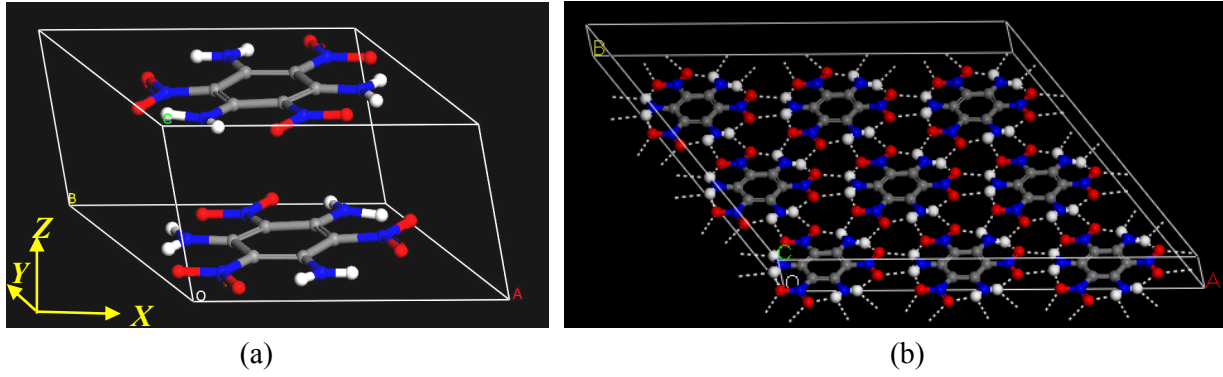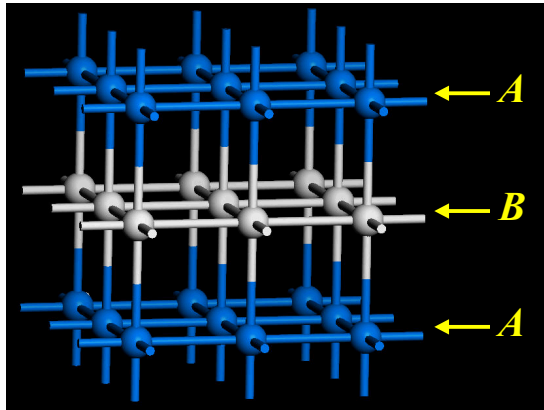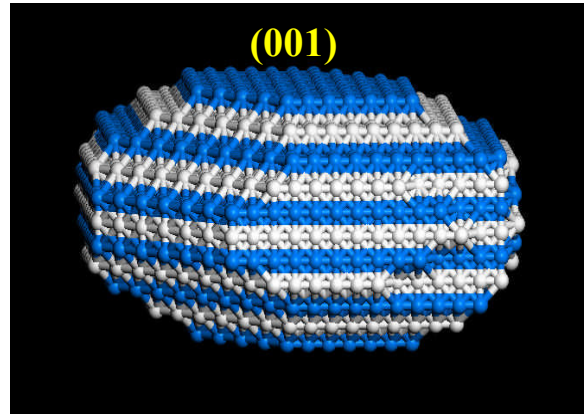
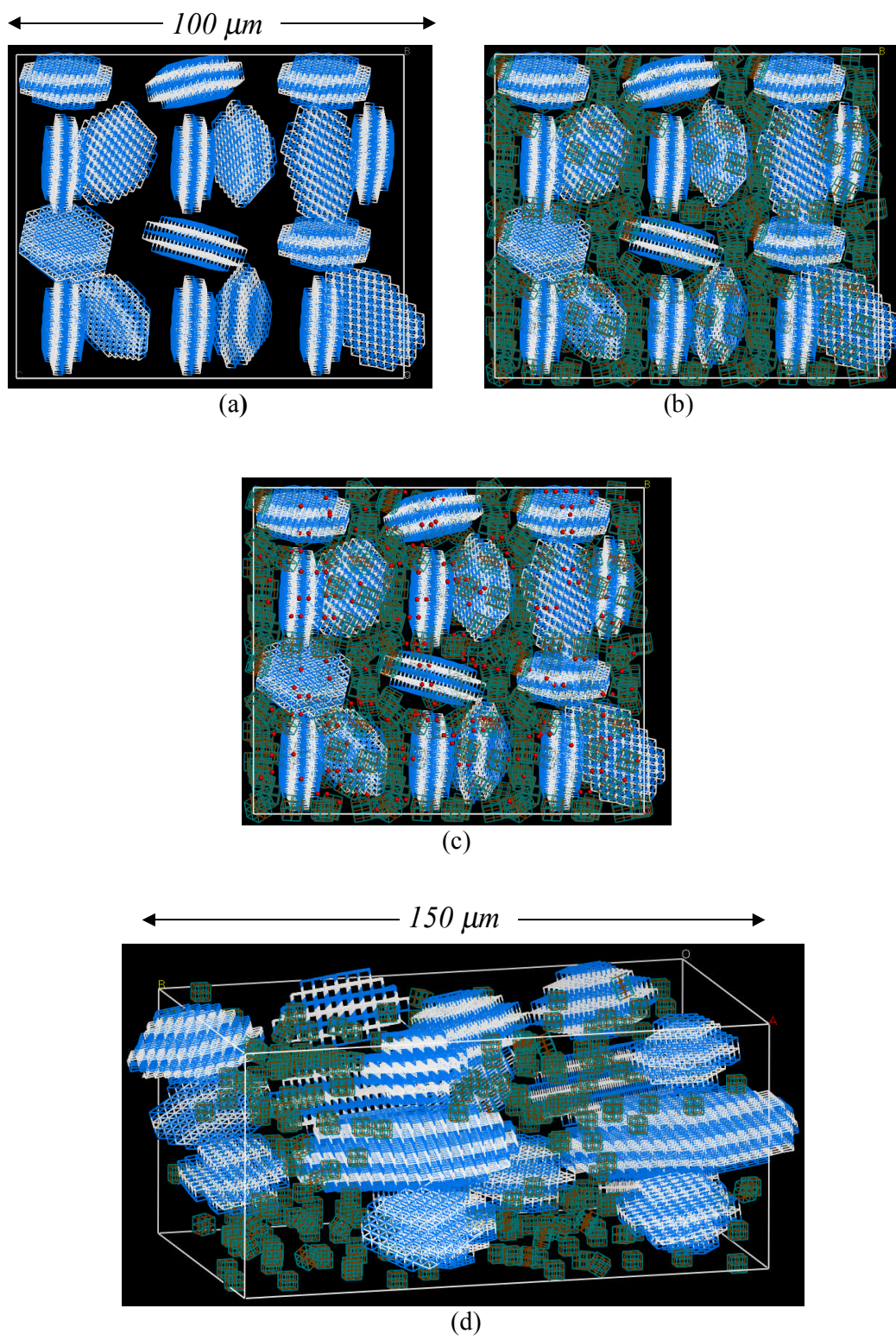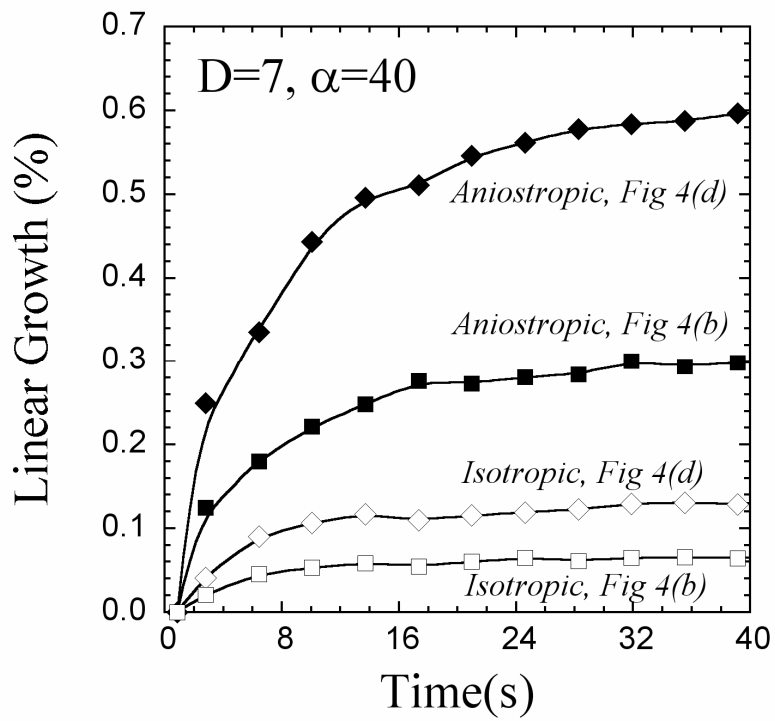(a)

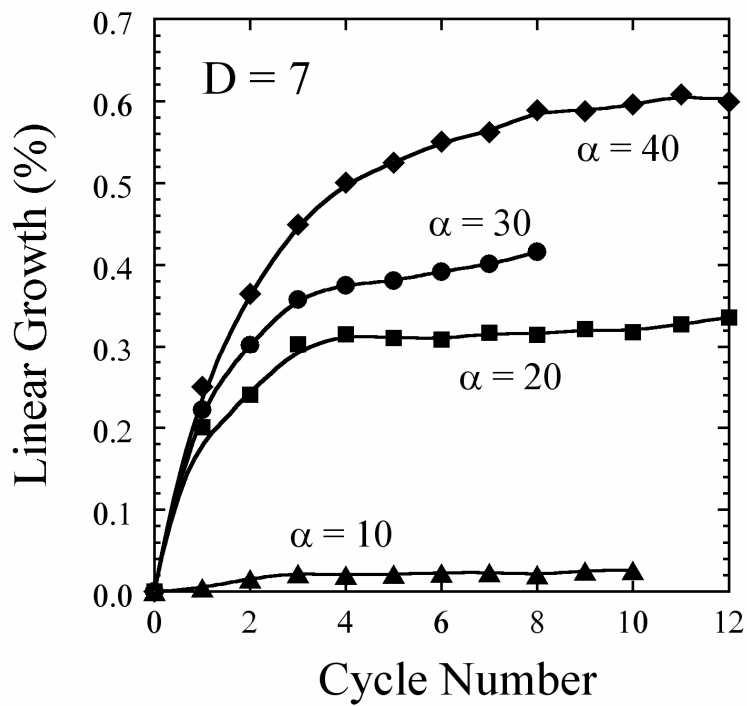(b)

Figure 1

(a)

(b)

(c)
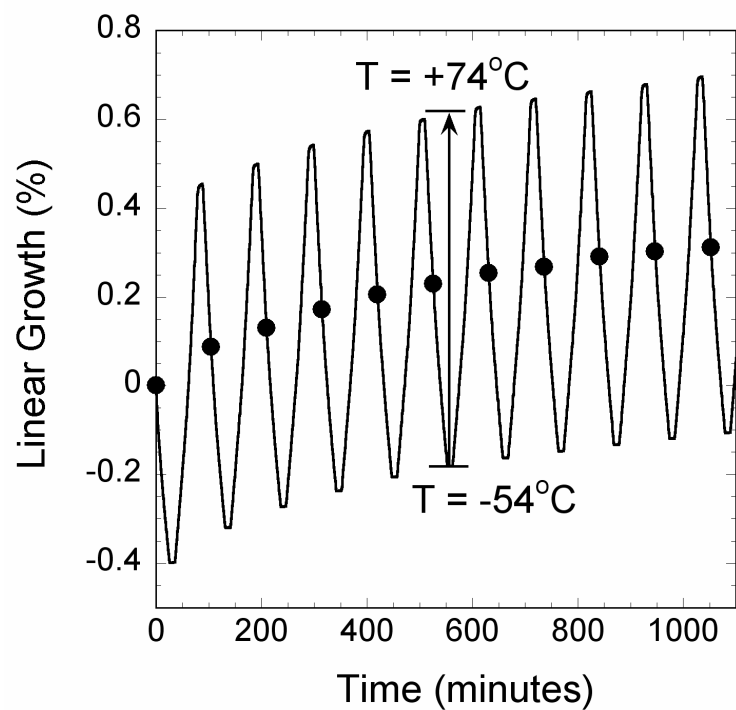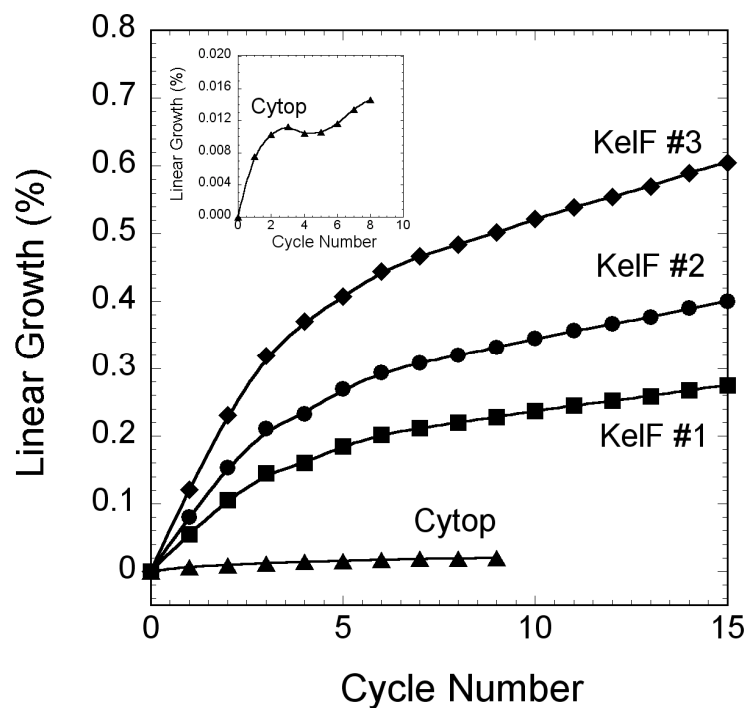
Figure 2

(a)

(b)

Figure 3

(a)

(b)

(c)

(d)

Figure 4

(a)

(b)

Figure 5

Figure 6